TU Delft

Delft University of Technology

Fast calculation of microphone array steering vectors with shear flow

Sijtsma, Pieter

Publication date
2018

Document Version
Accepted author manuscript

Published in
Proceedings of the 7th Berlin Beamforming Conference

Citation (APA)
Sijtsma, P. (2018). Fast calculation of microphone array steering vectors with shear flow. In *Proceedings of the 7th Berlin Beamforming Conference* Article BeBeC-2018-S3

Important note
To cite this publication, please use the final published version (if applicable).
Please check the document version above.

Copyright
Other than for strictly personal use, it is not permitted to download, forward or distribute the text or part of it, without the consent of the author(s) and/or copyright holder(s), unless the work is under an open content license such as Creative Commons.

Takedown policy
Please contact us and provide details if you believe this document breaches copyrights.
We will remove access to the work immediately and investigate your claim.

This work is downloaded from Delft University of Technology.
For technical reasons the number of authors shown on this cover page is limited to a maximum of 10.

FAST CALCULATION OF MICROPHONE ARRAY STEERING VECTORS WITH SHEAR FLOW

Pieter Sijtsma[1,2]
[1] PSA3, Prinses Margrietlaan 13, 8091 AV, Wezep, The Netherlands
[2] Faculty of Aerospace Engineering, TU Delft, The Netherlands

ABSTRACT

This paper proposes a fast method for calculating the acoustic time delay between an observer and a receiver in a shear flow. This method is applied to an outdoor microphone array measurement on a large-scale wind turbine. In such a set-up, a shear flow represents the actual wind field better than a uniform flow. Steering vectors for beamforming can be obtained by calculating the time delay between each point on a scan grid and each microphone. It is argued that omission in the steering vectors of the decay due to spherical spreading is preferable. Beamforming images show the benefits of ignoring the spherical spreading and of using a shear flow model. It is demonstrated that a shear flow model can also be used in combination with rotating source beamforming, again leading to beamforming improvements.

1 INTRODUCTION

Frequency-domain beamforming algorithms for microphone arrays [1] make use of so-called steering vectors, the elements of which describe the assumed acoustic propagation from a potential source to the microphones. Basically, the steering vector elements include the phase shift between the sound emitted by the source and the signal recorded by the microphone and, optionally, the attenuation caused by spherical spreading with respect to the sound level at a reference distance from the source.

The phase shift between source and microphone is directly related to the acoustic travel time between both, i.e., by multiplying the latter with the angular frequency. Thus, an accurate estimation of the travel time is indispensable for successful beamforming applications.

For beamforming in quiescent air, the travel time can easily be calculated by dividing the source-microphone distance by the speed of sound. If there is a uniform wind flow, as in a wind tunnel, the travel time can be calculated directly as well, by considering the distance between the microphone and the virtual source, which is displaced in flow direction from the true source during the same travel time.

If the flow is non-uniform, as in an open jet wind tunnel or outdoors, travel time calculations become more complicated. For shear flows, an obvious approach is the use of the ray tracing differential equations [2] to determine the acoustic path from source to microphone. Such a calculation starts with an estimated emission direction from the source, and the acoustic path obtained will usually not hit the microphone exactly. Therefore, an

iterative process is required to determine the precise path from source to microphone. This needs to be done for each potential source of the scan grid and for each microphone of the array. All in all, many ray tracing calculations are required, leading to long computation times. An interpolation approach proposed by Sarradj [3] leads to a significant acceleration of the process, but still the computation time is significant.

This paper proposes an alternative method for calculating the travel time, which is fully compatible with ray tracing but much faster. In this new method, the travel time is directly calculated by a numerical integration approach. The method is combined with an efficient iteration strategy to quickly determine the correct emission direction from the source. When coded in Fortran, the new method can calculate in a relatively short time (seconds rather than minutes) the travel times between all points in a typical scan grid and all microphones in a typical array.

In a shear flow the flow direction is constant, but the flow speed may vary in a direction perpendicular to the flow. Likewise, the temperature may vary in the same direction. This makes the method particularly suitable for outdoor wind turbine array measurements [4]. The merits of the method will be discussed using a wind turbine measurement recently carried out by Goldwind Asia.

In Section 2 of this paper the wind turbine test set-up is briefly described. Section 3 discusses the beamforming essentials and the benefit of ignoring spherical spreading. In Section 4 the new time delay integration method is presented and applied to the measurement. Section 5 discusses the application to rotating sources. The conclusions are summarised in Section 6.

2 TEST SET-UP

In March 2016, acoustic measurements were performed on a 3-bladed, 2.5 MW wind turbine of 90 m nacelle height. The measurements were carried out with an array of 80 microphones on the ground, at a view angle of approximately 45° towards the nacelle. Both upwind and downwind test conditions were considered.

A sketch of the upwind configuration can be found in Fig. 1. The tower height is 90 m and the rotor diameter 121 m. The cone angle of the rotor is 3° and the tilt angle 5°.

The distance between the centre of the microphone array and the tower axis is 95 m. Therefore, using a Cartesian coordinate system (x, y, z), with its origin in the array centre, the tower axis is at $(x, y) = (-95, 0)$. The distance between the tower centre line and the rotor plane is approximately 3 m. Hence, the distance between rotor and array centre is approximately 92 m in upwind configuration and 98 m in downwind configuration.

Here we consider a typical upwind measurement. The wind speed and temperature measured at the nacelle were 13.2 m/s (in negative x-direction) and 17.9 °C, respectively. The rotation speed was 13.5 RPM. The trailing edges of the blades were equipped with serrations.

The microphone array was 8 m long and 4 m wide and consisted of 80 MEMS microphones, arranged in concentric ellipses (see Fig. 2). The array was stretched in the x-direction to compensate for the fact that both the array and the rotor plane were at an angle of approximately 45° to the line of sight between the array centre and the nacelle. This should minimize the deformation of the beamforming main lobes, when the rotor plane is scanned.

Array measurements were done using a 65536 Hz sampling rate. The acquisition time was 10 s.

3 FREQUENCY DOMAIN BEAMFORMING

3.1 General expressions

Frequency-domain beamforming is usually done by averaging microphone signals that are corrected for phase delay and spherical spreading with respect to points in a scan grid. For example, in a uniform flow $U\vec{e}_x$ the acoustic response in $\vec{x}=(x,y,z)$ to a source of unit strength in a scan point $\vec{\xi}=(\xi,\eta,\zeta)$ can be expressed as [1]:

$$G(\vec{x},\vec{\xi})=\frac{1}{4\pi r_1(\vec{x},\vec{\xi})}\exp\left(-i\omega\tau(\vec{x},\vec{\xi})\right), \tag{1}$$

where ω is the angular frequency and $\tau(\vec{x},\vec{\xi})$ is the time delay:

$$\tau(\vec{x},\vec{\xi})=\frac{-M(x-\xi)+r_1(\vec{x},\vec{\xi})}{c\left(1-M^2\right)}. \tag{2}$$

Further, c is the sound speed, M is the Mach number:

$$M=U/c \tag{3}$$

and

$$r_1=\sqrt{\left(x-\xi\right)^2+\left(1-M^2\right)\left[\left(y-\eta\right)^2+\left(z-\zeta\right)^2\right]}. \tag{4}$$

Source amplitudes $a(\vec{\xi})$ can be obtained by "Delay-and-Sum" beamforming:

$$a(\vec{\xi})=\frac{1}{N}\sum_{n=1}^{N}p_n(\omega)\frac{r_1(\vec{x}_n,\vec{\xi})}{R_{\text{ref}}}\exp\left(i\omega\tau(\vec{x}_n,\vec{\xi})\right), \tag{5}$$

where $\vec{x}_n$ are the positions of the microphones, N is the number of microphones, $p_n(\omega)$ are the Fourier-transformed pressures and R_{ref} is a reference distance. Another, more often used method is "Conventional Beamforming" [1]:

$$a(\vec{\xi})=\frac{\sum_{n=1}^{N}p_n(\omega)\frac{R_{\text{ref}}}{r_1(\vec{x}_n,\vec{\xi})}\exp\left(i\omega\tau(\vec{x}_n,\vec{\xi})\right)}{\sum_{n=1}^{N}\frac{R_{\text{ref}}^2}{r_1(\vec{x}_n,\vec{\xi})^2}}. \tag{6}$$

Final beamforming results are obtained by squaring and averaging Eq. (5) or Eq. (6), yielding double summations featuring cross-spectra:

$$C_{mn}(\omega)=\frac{1}{2}\left\langle p_m(\omega)p_n^*(\omega)\right\rangle, \tag{7}$$

where the brackets stand for time averaging. Auto-spectra $C_{nn}(\omega)$ are often omitted from the double summation, as they can contain relatively much incoherent noise. This is also done in the present study.

3.2 Omission of spherical spreading

Results obtained with Conventional Beamforming, at a series of 1/3 octave band frequencies, are shown in Fig. 3. The reference distance R_{ref} was equal to the distance between the rotor hub and the array centre. The scan plane consisted of 6221 points on a disc of 140 m diameter. The grid resolution (distance between neighbouring grid points) was approximately 1.5 m. The disc geometry was adjusted to the cone and the tilt angle of the rotor blades.

A uniform flow was assumed at 7/8th of the wind speed at nacelle height (13.2 m/s). This is the average flow speed between the ground and the nacelle, when the standard 1/7th power law is used to describe the relation between wind speed and altitude.

At the lowest frequencies, the beamforming peak levels seem to be located above the rotor plane, which is not physical. The reason for this is the correction for spherical spreading made in Eq. (6). This causes the beamforming levels to increase when the scan point moves upwards from the true source positions, since the effect of correction for spherical spreading is larger than the effect of source mismatch.

When the aim is to locate sources in a set-up like discussed in this paper (scan plane perpendicular to array plane), it is better to omit the correction for spherical spreading. That is: $r_1(\vec{x}_n, \vec{\xi})$ in Eqs. (6) and (7) should be replaced by R_{ref}. In either case, the following beamforming expression remains:

$$a(\vec{\xi}) = \frac{1}{N}\sum_{n=1}^{N} p_n(\omega)\exp\left(i\omega\tau(\vec{x}_n, \vec{\xi})\right). \tag{8}$$

With this beamforming expression, the results must be interpreted as “as measured by the array”.

Another reason for omitting the correction for spherical spreading is that it assumes acoustic sources with omnidirectional radiation, whereas true wind turbine aeroacoustic sources are not omnidirectional at all. Moreover, the source directivity depends on blade modifications aiming at reducing the noise emission, such as trailing edge serrations.

Results of beamforming without correction for spherical spreading are shown in Fig. 4. Now the peak level locations are all within the rotor disc. This is confirmed by Fig. 5, which shows the radial peak level locations.

In the remaining part of this paper, all beamforming results are without correction for spherical spreading.

4 CORRECTION FOR SHEAR FLOW

4.1 Shear flow effects

In the previous chapter, beamforming was done under the assumption of a uniform flow with speed 11.55 m/s, which is 7/8th of the wind speed at the nacelle. Assuming a 1/7th power law, the actual wind speed at the highest rotor location (150 m) is 14.20 m/s. So, for beamforming on points at that altitude, a uniform flow speed of 12.42 m/s (7/8×14.20) would have been more appropriate. Thus, an error of 0.87 m/s is made. The acoustic time delay to the centre of the array is 0.515 s, which corresponds to an error of 0.45 m in the virtual source position. The corresponding source location error on the array plane is (150/92)×0.45 =

0.73 m. Likewise, at the lowest rotor location (30 m), the source location error on the array plane is approximately 0.15 m, but in the other direction.

Although the location errors made with the assumption of uniform flow are not very large, and within the spatial resolution of the scan grid, it can be beneficial to include the altitude-dependency of the wind speed in the calculation of the time delay from scan point to microphone. This can be done by using the ray tracing differential equations [2]. However, this is rather time-consuming [3], even in combination with an interpolation method.

Therefore, a different approach is followed here, featuring a combination of a direct calculation of the time delay and an efficient shooting strategy. These two aspects are detailed in the following sections.

4.2 Time delay calculation

Suppose that the acoustic path from a source location $\vec{\xi}$ to a microphone location $\vec{x}$ is described by

$$\vec{s}(h) = \big(f(h), g(h), h \big), \tag{9}$$

with

$$\begin{cases} \vec{\xi} = \vec{s}(\zeta) = \big(f(\zeta), g(\zeta), \zeta \big), \\ \vec{x} = \vec{s}(z) = \big(f(z), g(z), z \big). \end{cases} \tag{10}$$

Using this parametrisation of the acoustic path, we will derive an integral to calculate the time delay. The integration parameter h (the height) runs from $h = \zeta$ to $h = z$. Note that $dh < 0$ when the source location is above the microphone.

In a uniform flow $U\vec{e}_x$ the time delay from a source location $\vec{\xi}$ to a microphone location $\vec{x}$ is given by Eqs. (2) and (4):

$$\tau = \frac{1}{c\left(1-M^2\right)}\left(-M(x-\xi) + \sqrt{(x-\xi)^2 + \left(1-M^2\right)\left[(y-\eta)^2 + (z-\zeta)^2 \right]} \right). \tag{11}$$

Likewise, in a small layer of height $|dh|$, the time delay from $\vec{s}(h)$ to $\vec{s}(h+dh)$ is

$$d\tau = \frac{dh}{c\left(1-M^2\right)}\left(-Mf'(h) + \lambda\sqrt{f'(h)^2 + \left(1-M^2\right)\left(g'(h)^2+1\right)} \right), \tag{12}$$

where λ is the sign of dh. Thus, the total time delay in a non-uniform shear flow is given by

$$T(f,g) = \int_{\zeta}^{z} \frac{1}{c(h)\left(1-M(h)^2\right)}\left(-M(h)f'(h) + \lambda\sqrt{f'(h)^2 + \left(1-M(h)^2\right)\left(g'(h)^2+1\right)} \right) dh\,. \tag{13}$$

The functions f and g should describe the fastest path from $\vec{\xi}$ to $\vec{x}$, which means that

$$T(f+\varepsilon, g+\delta) - T(f,g) = 0\,, \tag{14}$$

for all infinitesimally small and continuously differentiable functions ε and δ with

$$\varepsilon(\zeta) = \delta(\zeta) = \varepsilon(z) = \delta(z) = 0\,. \tag{15}$$

Insertion of Eq. (14) in Eq. (13) yields

$$\int_{\varsigma}^{z} \frac{1}{c(h)\left(1-M(h)^2\right)}\left(-M(h)\varepsilon'(h)+\lambda\frac{f'(h)\varepsilon'(h)+\left(1-M(h)^2\right)g'(h)\delta'(h)}{\sqrt{f'(h)^2+\left(1-M(h)^2\right)\left(g'(h)^2+1\right)}}\right)dh=0. \quad (16)$$

Integration by parts, while using Eq. (15), gives

$$\int_{\varsigma}^{z}\left\{\varepsilon(h)\frac{d}{dh}\left[\frac{1}{c(h)\left(1-M(h)^2\right)}\left(-M(h)+\lambda\frac{f'(h)}{\sqrt{f'(h)^2+\left(1-M(h)^2\right)\left(g'(h)^2+1\right)}}\right)\right]\right. \\ \left.+\delta(h)\frac{d}{dh}\left[\frac{1}{c(h)\left(1-M(h)^2\right)}\left(\lambda\frac{\left(1-M(h)^2\right)g'(h)}{\sqrt{f'(h)^2+\left(1-M(h)^2\right)\left(g'(h)^2+1\right)}}\right)\right]\right\}dh=0. \quad (17)$$

Since Eq. (17) must be true for any function ε and δ, we must have

$$\begin{cases}\dfrac{1}{c(h)\left(1-M(h)^2\right)}\left(-M(h)+\lambda\dfrac{f'(h)}{\sqrt{f'(h)^2+\left(1-M(h)^2\right)\left(g'(h)^2+1\right)}}\right)=C_1,\\ \dfrac{g'(h)}{c(h)\sqrt{f'(h)^2+\left(1-M(h)^2\right)\left(g'(h)^2+1\right)}}=C_2,\end{cases} \quad (18)$$

which is essentially the continuous version of Snell's Law.

The constants C_1 and C_2 in Eq. (18) are obtained by inserting the start value $h=\zeta$ and a "shoot" vector $\left(f'(\zeta),g'(\zeta),\lambda\right)$. For other values of *h*, $f'(h)$ and $g'(h)$ can explicitly be derived from Eq. (18), as detailed in Appendix A. Then, the time delay is obtained by numerically evaluating Eq. (13), which can be done efficiently using Romberg's method. The endpoint $\vec{x}$ is also obtained numerically:

$$\begin{cases}\xi=x+\int_{z}^{\zeta}f'(h)dh,\\ \eta=y+\int_{z}^{\zeta}g'(h)dh.\end{cases} \quad (19)$$

Note that Romberg's method assumes the integrands to be infinitely continuously differentiable, which means that a power law for the wind speed cannot be applied down to $h=0$ (i.e., the ground). Instead, a piecewise linear profile can be used, while integrating piece by piece.

4.3 Shooting procedure

The endpoint $\vec{x}$ obtained by the integration method described in the previous section depends on the initial shoot vector $\left(f'(\zeta),g'(\zeta),\lambda\right)$. To reach a targeted endpoint $\vec{x}^{(0)}$ (i.e., microphone position), one needs to start with the appropriate shoot vector. This vector can be obtained with an iteration procedure, introducing the "shoot direction":

$$\vec{w}^{(i)} = \frac{\left(f'(\zeta), g'(\zeta), \lambda\right)}{\left\|\left(f'(\zeta), g'(\zeta), \lambda\right)\right\|} \;\Leftrightarrow\; \left(f'(\zeta), g'(\zeta), \lambda\right) = \frac{\vec{w}^{(i)}}{\left|w_z^{(i)}\right|} \tag{20}$$

($w_z^{(i)}$ being the *z*-component of $\vec{w}^{(i)}$) and the "view direction"

$$\vec{v}^{(i)} = \frac{\vec{x}^{(i)} - \vec{\xi}}{\left\|\vec{x}^{(i)} - \vec{\xi}\right\|}, \tag{21}$$

where $\vec{x}^{(i)}$ is the most recently found endpoint. Initial values are

$$\vec{w}^{(1)} = \vec{v}^{(0)} = \frac{\vec{x}^{(0)} - \vec{\xi}}{\left\|\vec{x}^{(0)} - \vec{\xi}\right\|}. \tag{22}$$

At each iteration step the shoot direction is corrected with respect to the previous one by an angle equal to the mismatch between the actual view direction $\vec{v}^{(i)}$ and the desired view direction $\vec{v}^{(0)}$:

$$\vec{w}^{(i+1)} = \left(\vec{v}^{(0)} \cdot \vec{v}^{(i)}\right)\vec{w}^{(i)} - \left(\vec{v}^{(0)} \times \vec{v}^{(i)}\right) \times \vec{w}^{(i)}. \tag{23}$$

With this, only a few iterations are required for obtaining a converged solution.

4.4 Implementation

The shooting and integration method described in the previous sections was implemented in a Fortran routine, and run on a laptop with Intel Core i7 processor @ 2.2 GHz. The computation time for calculating the time delays between all 80 microphones and all 6221 grid points was less than 10 s.

The 1/7th power law wind profile was approximated by a piecewise linear profile. The wind speed was specified at the following altitudes: 2 m, 5 m, 10 m, 20 m, 50 m, 100 m and 200 m. Results were compared with the traditional ray tracing method [2], yielding exact agreement.

Beamforming images are shown in Fig. 6, which is quite similar to Fig. 4, except that the source spots in the upper half of the rotor disc moved a little upward. The extended source regions seem to be better aligned with the circles in the rotor disc. Note that the scan grid was adjusted somewhat in *x*-direction, such that maximum beamforming output was found. This was also done for the uniform flow case (Fig. 4). There was a 3 m difference in axial scan grid location between the uniform and the shear flow case.

Radial peak level locations, for uniform and shear flow, are shown in Fig. 7. There is not much difference between both cases, except that the locations found with shear flow are more constant at high frequencies.

5 APPLICATION TO ROTATING SOURCES

Without much effort, the shear flow time delay results can be applied also to beamforming on rotating sources. This can be done by properly arranging the scan grid, namely as a set of concentric rings that follow the rotating motion. The scan grid used for the present study was arranged this way, see Fig. 8. For such a grid, the time delays only need to be calculated for the base scan grid. When the grid points rotate, so their locations become time-dependent, the time delay at each point in time can be obtained by linear interpolation using the nearest base

grid points on the same ring. Obviously, the grid resolution needs to be fine enough in relation to the maximum frequency to be analysed. A grid refinement study confirmed that the present scan grid was sufficiently fine for beamforming up to 4000 Hz.

Beamforming on rotating sources was done with the ROSI method [5], which features a straightforward time-domain Delay-and-Sum method to reconstruct source signals $\sigma(t)$ in scan points $\vec{\xi}$. Without atmospheric decay, the Delay-and-Sum method reads

$$\sigma(t) = \frac{1}{N}\sum_{n=1}^{N} \chi_n\left(t + \tau\left(\vec{x}_n, \vec{\xi}(t)\right)\right). \tag{24}$$

where χ_n is the time signal recorded by the n^{th} microphone. Source powers were calculated following a procedure similar to ignoring microphone auto-spectra in conventional frequency-domain beamforming [5].

Beamforming results with uniform flow are shown in Fig. 9 and with shear flow in Fig. 10. With shear flow the levels are slightly higher, indicating a better agreement between propagation model and measurement. Nevertheless, the differences are small.

For both cases, radial peak level locations are shown in Fig. 11. Again, there is not much difference, but with shear flow the locations are more constant at high frequencies.

6 CONCLUSIONS

A fast method is proposed for calculating the acoustic time delay between points in a shear flow. With this, improved steering vectors can be obtained for beamforming through a non-uniform flow. The benefits were demonstrated using an outdoor array measurement on a large-scale wind turbine. The shear flow model can also be applied to, and is also beneficial for rotating source beamforming. The improvements with respect to uniform flow are moderate, but the additional computation time is moderate as well.

ACKNOWLEDGEMENT

The investigations reported in this paper were carried out under a contract with Goldwind.

APPENDIX A: EXPLICIT EXPRESSION FOR TANGENT OF ACOUSTIC PATH

In this appendix, explicit expressions are derived for $f'(h)$ and $g'(h)$, f and g describing the acoustic path from $\vec{\xi}$ to $\vec{x}$, see Eqs. (9) and (10). Starting point is Eq. (18), which is rewritten as

$$\begin{cases} \dfrac{f'(h)}{\sqrt{f'(h)^2 + \left(1-M(h)^2\right)\left(g'(h)^2+1\right)}} = A(h) = \lambda\left[M(h) + C_1 c(h)\left(1-M(h)^2\right)\right], \\ \dfrac{g'(h)}{\sqrt{f'(h)^2 + \left(1-M(h)^2\right)\left(g'(h)^2+1\right)}} = B(h) = C_2 c(h). \end{cases} \tag{25}$$

By squaring these equations, the following linear equations for $f'(h)^2$ and $g'(h)^2$ follow:

$$\begin{cases} \left(1-A(h)^2\right) f'(h)^2 - A(h)^2\left(1-M(h)^2\right) g'(h)^2 = \left(1-M(h)^2\right) A(h)^2, \\ -B(h)^2 f'(h)^2 + \left(1-B(h)^2\left(1-M(h)^2\right)\right) g'(h)^2 = \left(1-M(h)^2\right) B(h)^2. \end{cases} \tag{26}$$

The solution of Eq. (26) is

$$\begin{cases} f'(h)^2 = \dfrac{1-M(h)^2}{D(h)} A(h)^2, \\ g'(h)^2 = \dfrac{1-M(h)^2}{D(h)} B(h)^2, \end{cases} \tag{27}$$

with

$$D(h) = 1 - A(h)^2 - \left(1-M(h)^2\right) B(h)^2 = \frac{1-M(h)^2}{f'(h)^2 + \left(1-M(h)^2\right)\left(g'(h)^2+1\right)}. \tag{28}$$

From Eq. (25) follows, under the condition that $D(h) > 0$,

$$\begin{cases} f'(h) = \sqrt{\dfrac{1-M(h)^2}{D(h)}} A(h), \\ g'(h) = \sqrt{\dfrac{1-M(h)^2}{D(h)}} B(h). \end{cases} \tag{29}$$

Note that Eq. (13) can be simplified into

$$T(f,g) = \int_{\varsigma}^{z} \frac{f'(h)}{c(h)\left(1-M(h)^2\right)} \left(-M(h) + \frac{\lambda}{A(h)} \right) dh \,. \tag{30}$$

REFERENCES

[1] P. Sijtsma, “Acoustic beamforming for the ranking of aircraft noise.” In C. Schram, R. Dénos, and E. Lecomte (eds), “Accurate and Efficient Aeroacoustic Prediction Approaches for Airframe Noise.”, VKI Lecture Series 2013-03, March 25-29, 2013.

[2] A.D. Pierce, “Acoustics: An Introduction to Its Physical Principles and Applications”, Acoustical Society of America, 1989.

[3] E. Sarradj, “A fast ray casting method for sound refraction at shear layers”, Int. J. Aeroacoustics, 16, 65-77, 2017.

[4] S. Oerlemans, P. Sijtsma, and B. Méndez López, “Location and Quantification of Noise Sources on a Wind Turbine”, J. Sound Vib., 299, 869-883, 2007.

[5] P. Sijtsma, S. Oerlemans, and H. Holthusen, “Location of Rotating Sources by Phased Array Measurements”, AIAA 2001-2167, 2001, 7th CEAS/AIAA Aeroacoustics Conference, Maastricht, The Netherlands, 28-30 May 2001.

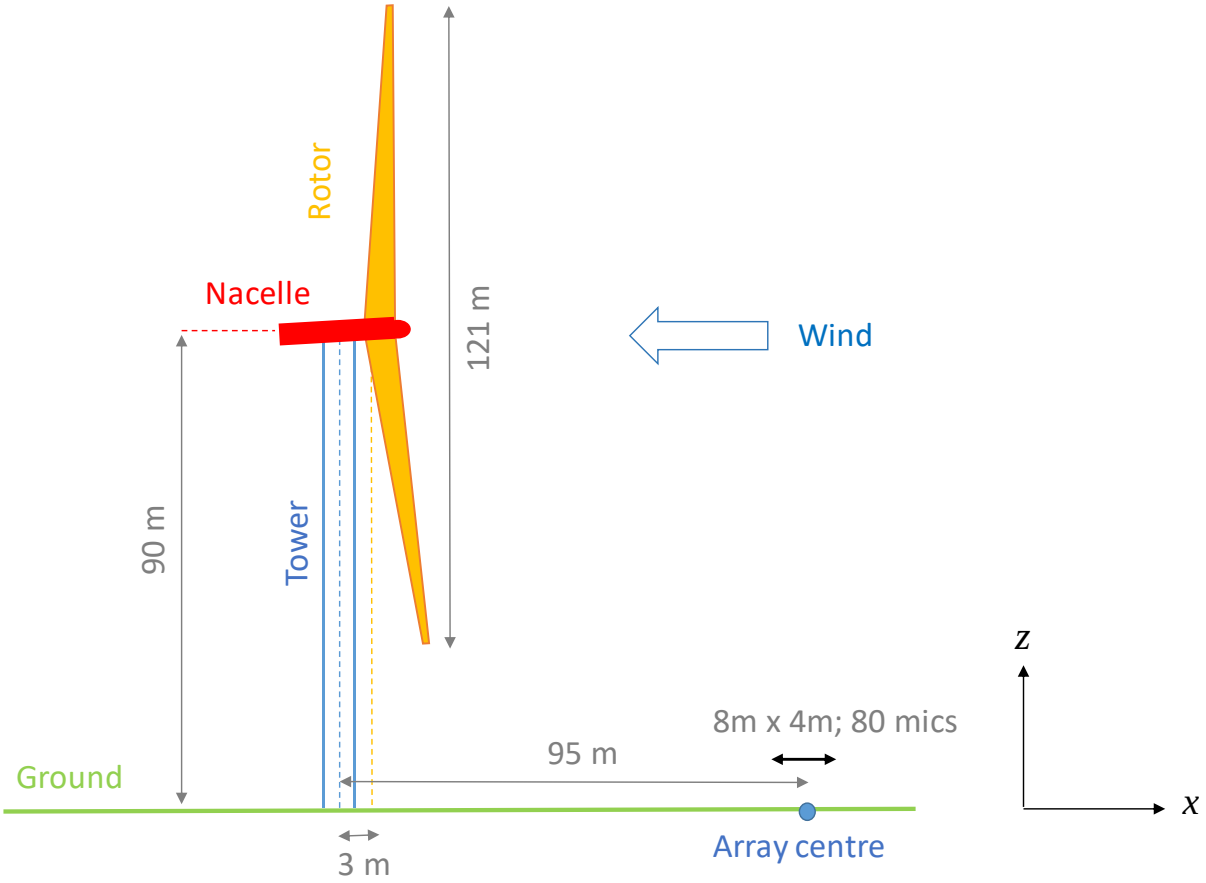

Fig. 1. Sketch of the measurement set-up.

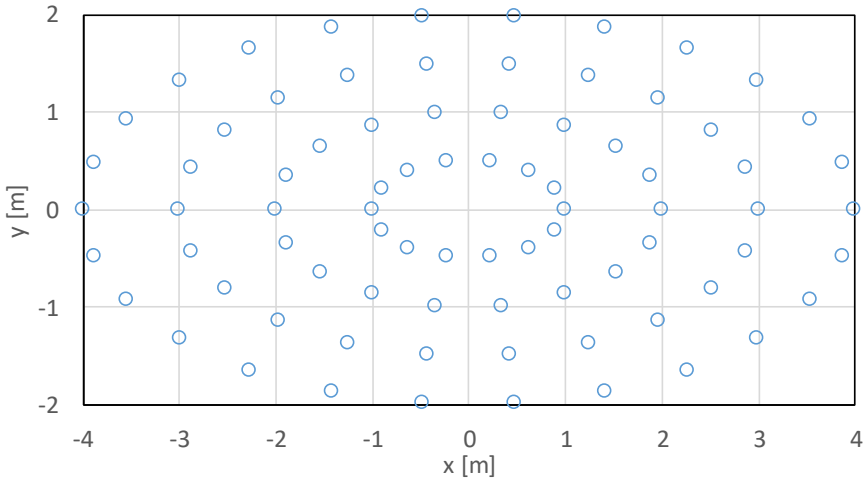

Fig. 2. Microphone array lay-out.

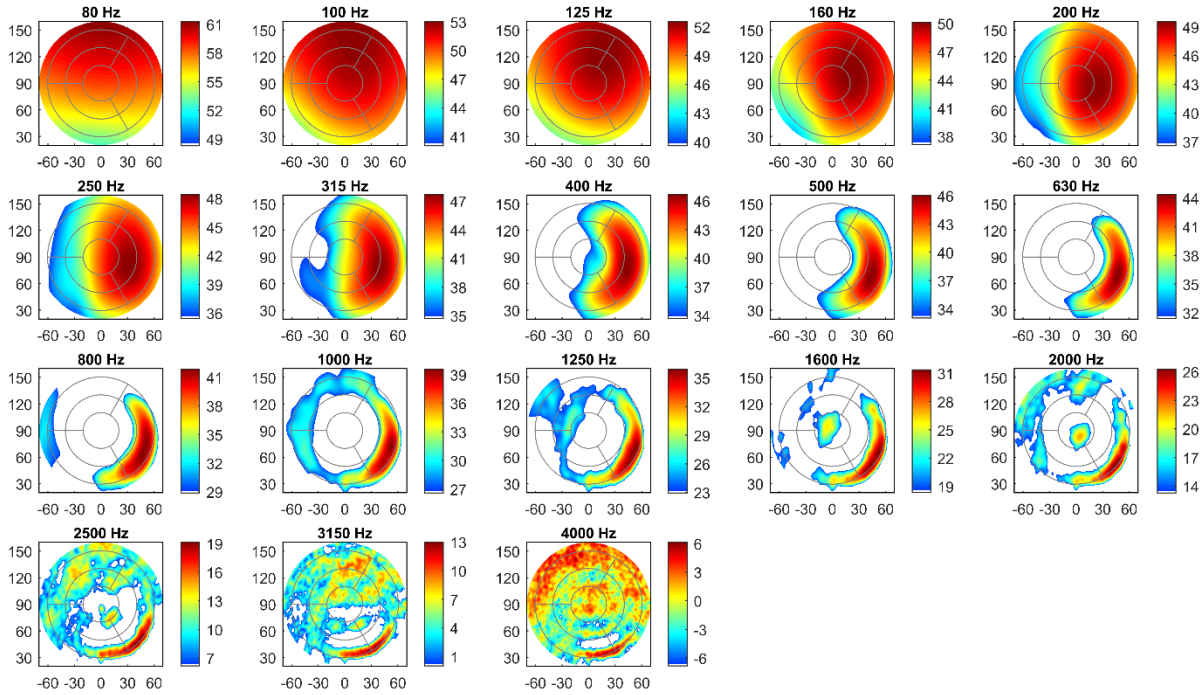

Fig. 3. Conventional Beamforming images, including corrections for spherical spreading.

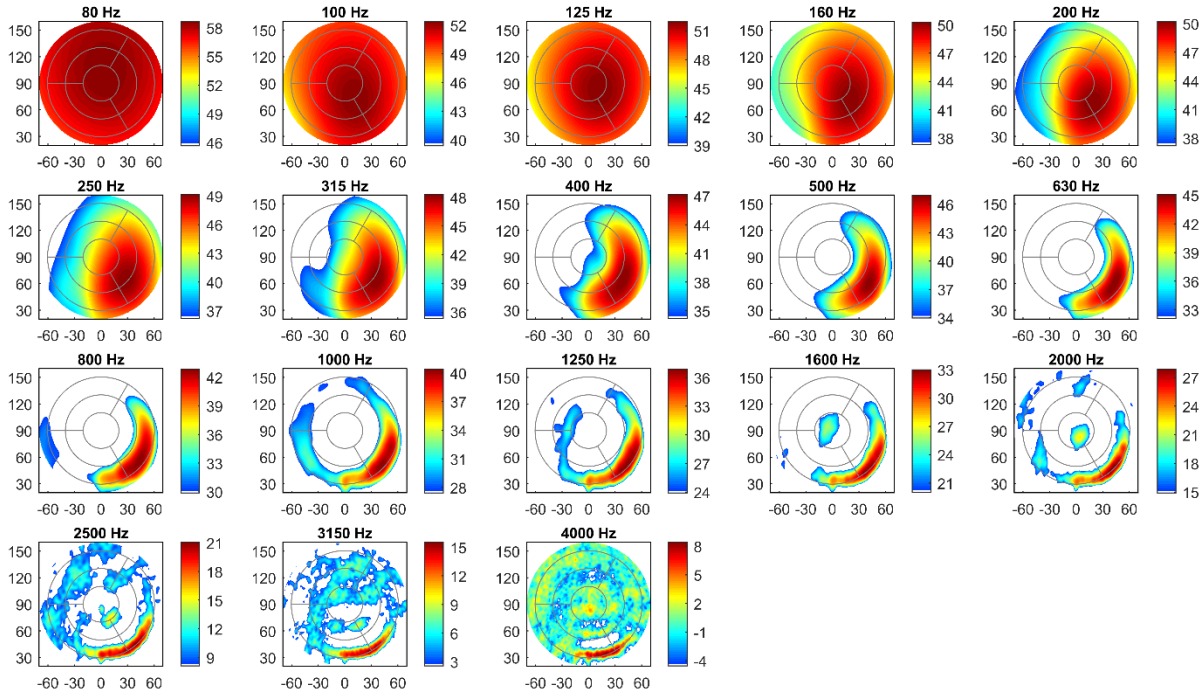

Fig. 4. Conventional Beamforming images, without corrections for spherical spreading.

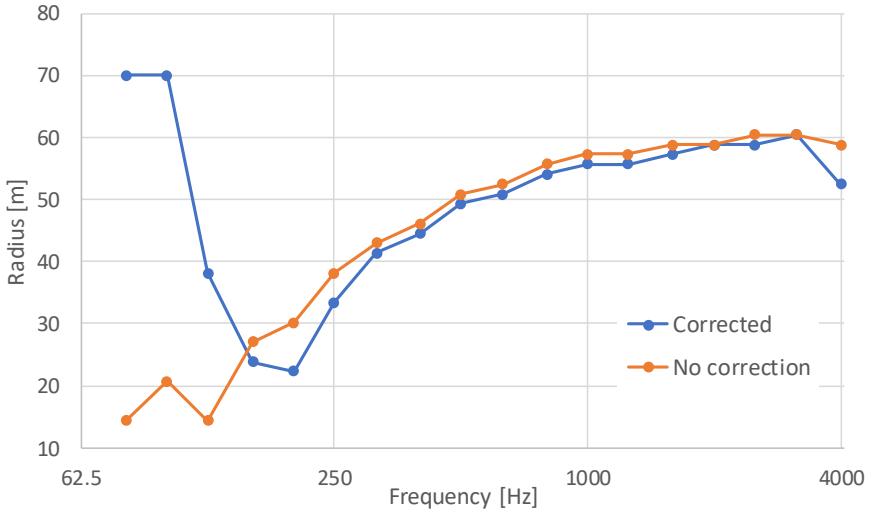

Fig. 5. Radial beamforming peak level locations, with and without correction for spherical spreading.

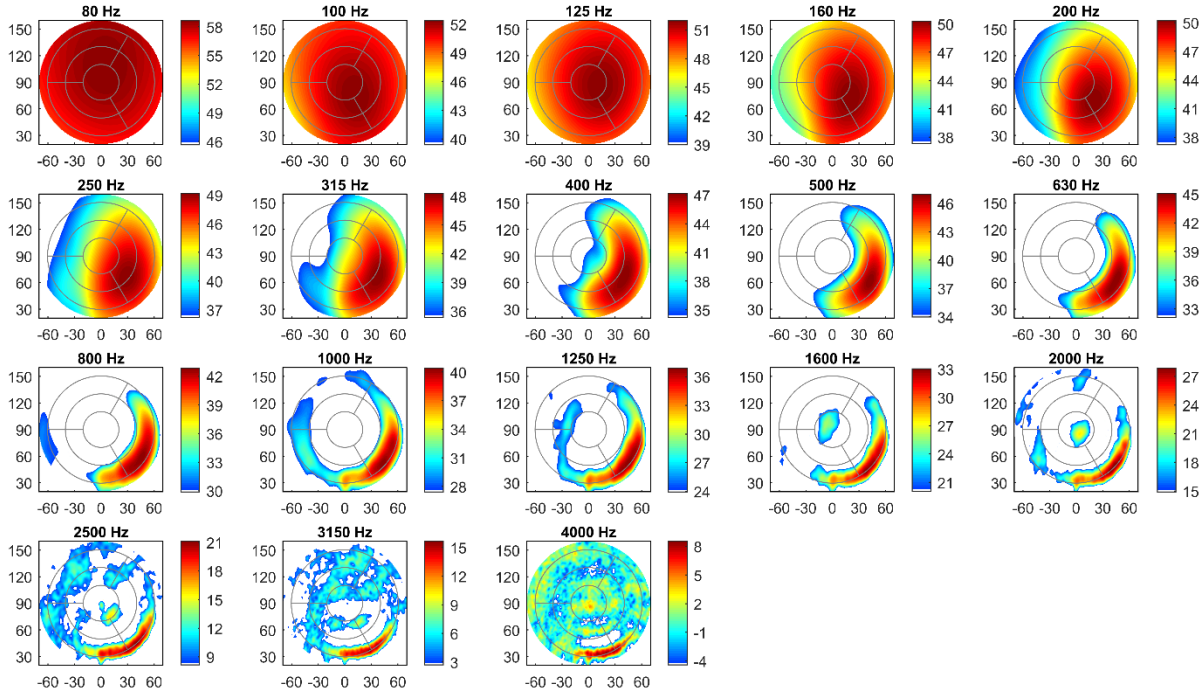

Fig. 6. Conventional Beamforming images, obtained with shear flow.

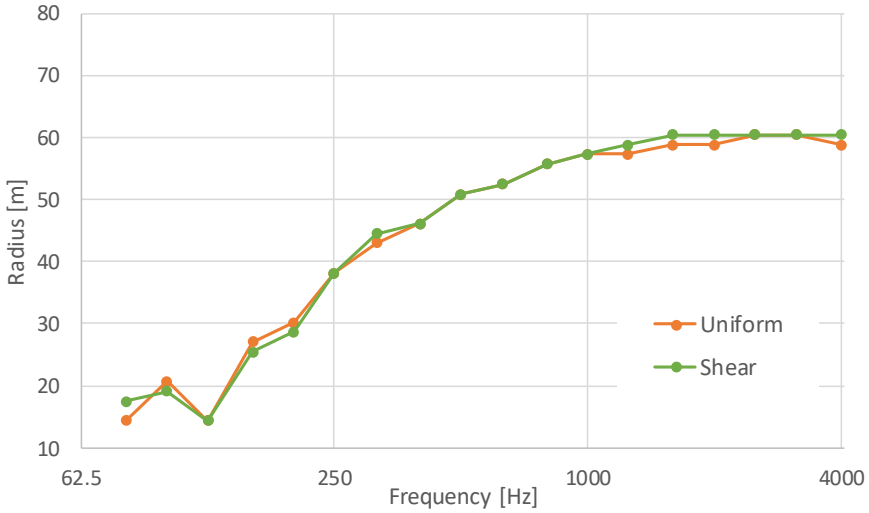

Fig. 7. Radial beamforming peak level locations, obtained with uniform and shear flow.

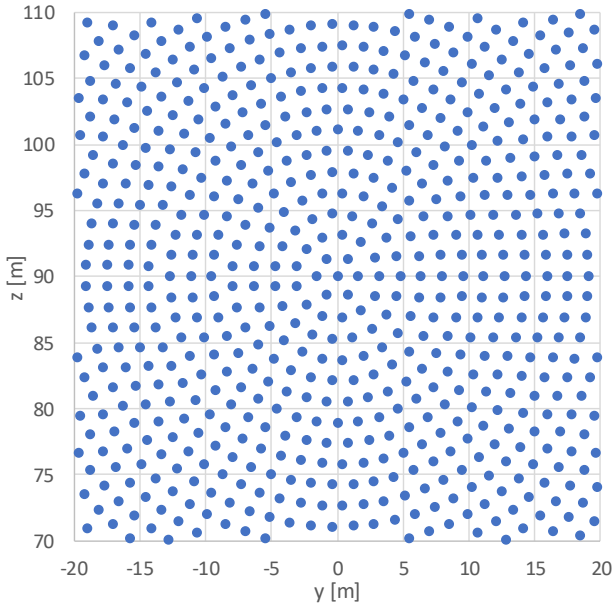

Fig. 8. Inner part of scan grid.

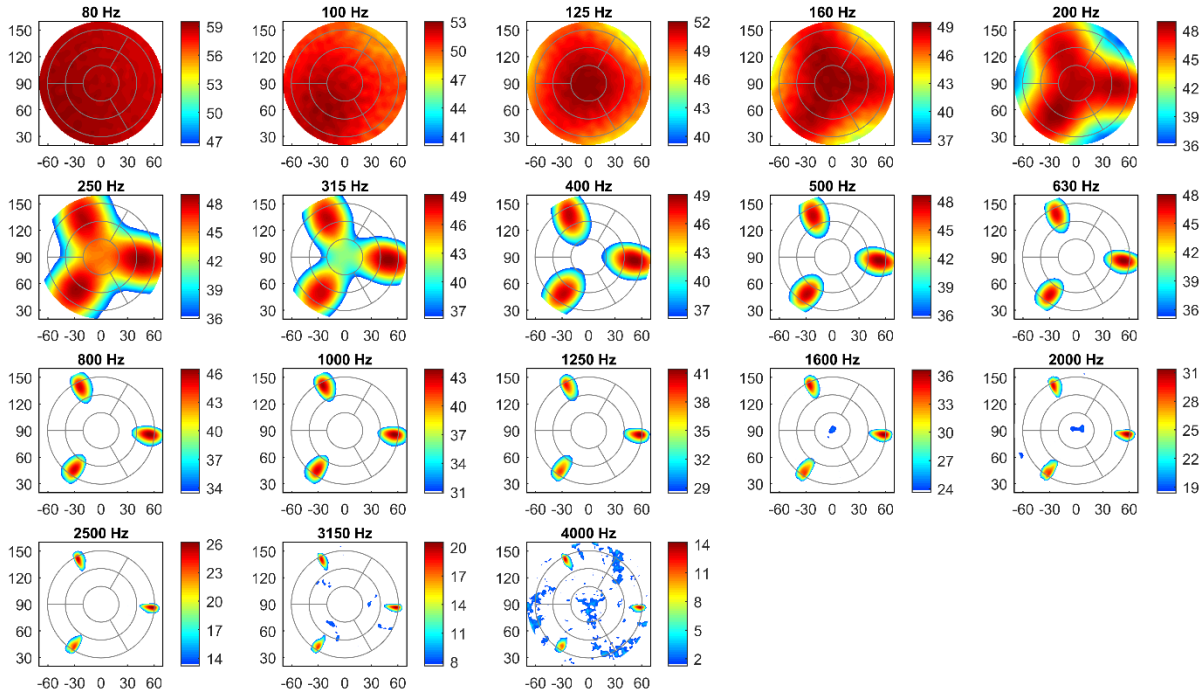

Fig. 9. ROSI beamforming images, obtained with uniform flow.

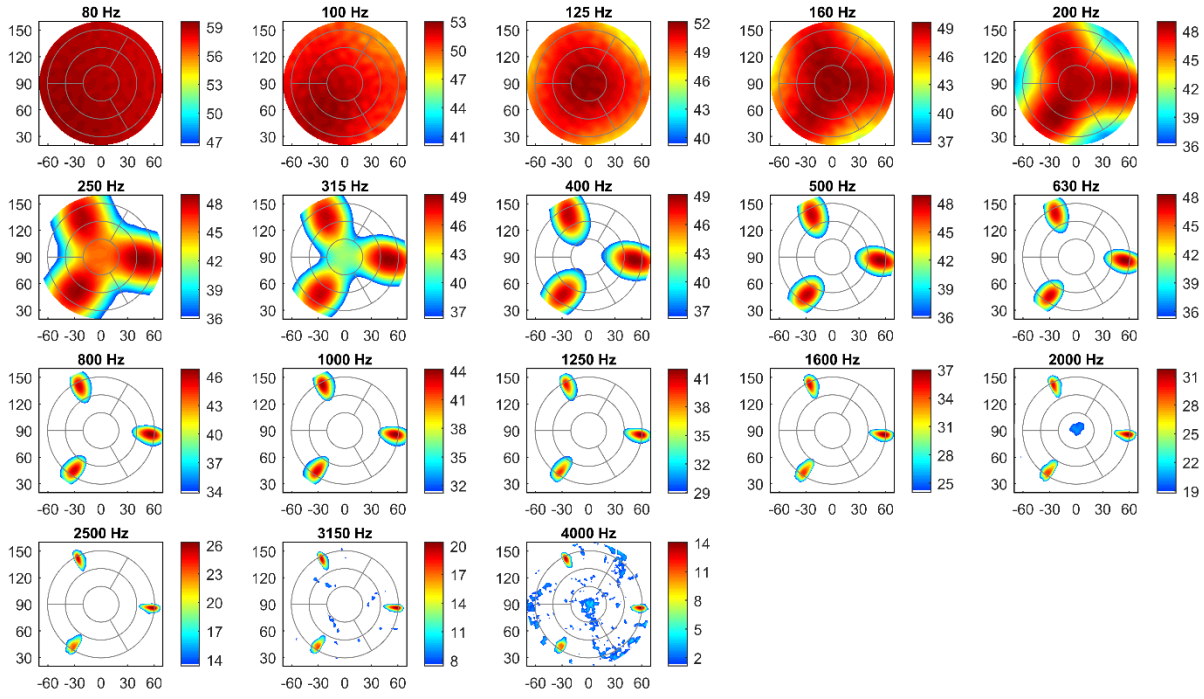

Fig. 10. ROSI beamforming images, obtained with shear flow.

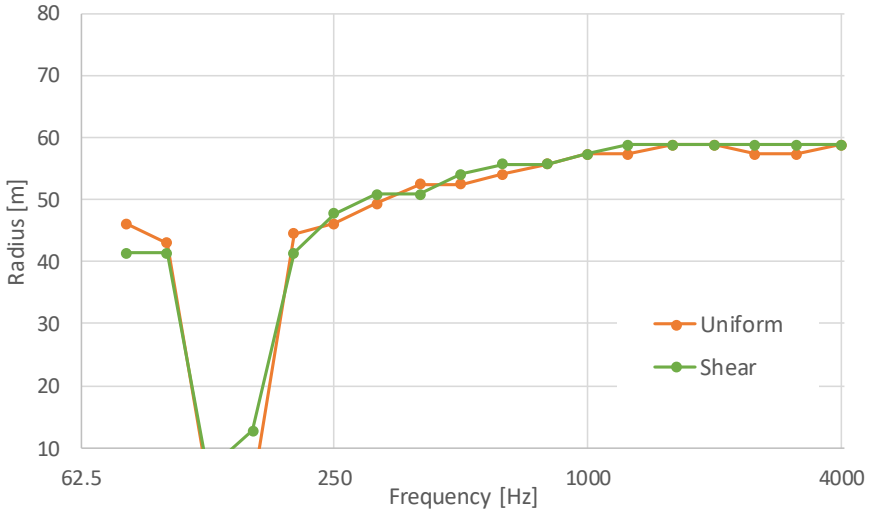

Fig. 11. ROSI radial peak level locations, obtained with uniform and shear flow.